Conductance stability in chaotic and integrable quantum dots with random impurities

Guanglei Wang,[1] Lei Ying,[1] and Ying-Cheng Lai[1,2]
[1]*School of Electrical, Computer, and Energy Engineering, Arizona State University, Tempe, Arizona 85287, USA*
[2]*Department of Physics, Arizona State University, Tempe, Arizona 85287, USA*
(Received 4 May 2015; revised manuscript received 30 June 2015; published 3 August 2015)

For a quantum dot system of fixed geometry, in the presence of random impurities the average conductance over an appropriate range of the Fermi energy decreases as the impurity strength is increased. Can the nature of the corresponding classical dynamics in the dot region affect the rate of decrease? Utilizing graphene quantum dots with two semi-infinite, single-mode leads as a prototypical model, we address the device stability issue by investigating the combined effects of classical dynamics and impurities on the average conductance over the energy range of the first transverse mode. We find that, for chaotic dot systems, the rate of decrease in the average conductance with the impurity strength is in general characteristically smaller than that for integrable dots. We develop a semiclassical analysis for the phenomenon and also obtain an understanding based on the random matrix theory. Our results demonstrate that classical chaos can generally lead to a stronger stability in the device performance, strongly advocating exploiting chaos in the development of nanoscale quantum transport devices.

DOI: 10.1103/PhysRevE.92.022901 PACS number(s): 05.45.Mt, 72.80.Vp, 73.23.−b, 73.63.−b

I. INTRODUCTION

In the development of nanoscale quantum devices, an important issue is stability against random perturbations such as various types of impurities. While the impurities can be reduced to certain extent through the improvement and refinement of the underlying fabrication process, it is of interest to uncover alternative mechanisms to enhance the device stability. The purpose of this paper is to show that classical chaos can be exploited to generate devices that are relatively more stable in the quantum regime than those exhibiting integrable dynamics in the classical limit.

To be concrete, we study quantum dot systems, an essential type of structures in nanoelectronic devices. Such a system consists of a central scattering region, or a dot region, and a number of electronic waveguides (leads). Incoming electrons from one lead undergo scattering in the dot region and become outgoing in all leads. For quantum dots a fundamental phenomenon is universal conductance fluctuations [1–5] with respect to variations in parameters such as the Fermi energy or the strength of an external magnetic field. In particular, for mesoscopic systems in the ballistic transport regime, at low temperatures the conductance fluctuations tend to be independent of the sample size and impurities [1] and thus can serve as a probe of quantum chaos [5], a field aiming to uncover and understand the quantum manifestations of classical chaos [6]. For over two decades quantum dot systems have become a paradigm to study quantum chaotic scattering [7,8], and there has been a large body of literature on the effects of distinct types of classical dynamics on conductance fluctuations [9–19]. A basic result is that, for systems with integrable or mixed classical dynamics, the conductance curves typically contain a large number of Fano resonances [20–24], leading to sharp conductance fluctuations. But if the system has fully developed classical chaos, conductance fluctuations will be smooth. This result enables conductance fluctuations to be modulated through the control of the underlying classical dynamics [25,26].

To address the problem of device stability with respect to random impurities, in this paper we shall not be concerned with conductance fluctuations. Instead, we consider ensemble of random impurities of systematically varying strength and investigate their effects on some *appropriately averaged value of the conductance*. For this purpose we consider quantum-dot systems of two semi-infinite leads, each supporting a *single* transverse mode, and focus on the average conductance over the corresponding single-mode Fermi-energy range. This energy range is classically small but quantum mechanically large, rendering applicable semiclassical treatment of the scattering dynamics [27]. To contrast the role of classical dynamics, we choose two types of geometric domains for the dot region: stadium and rectangle, which generate classical chaotic and integrable dynamics, respectively. As the strength of the random impurities is increased from zero, the average conductance will decrease due to localization of wave functions. However, we find that the integrable dot system exhibits a much faster decrease in the average conductance than that for the chaotic dot system, implying a stronger conductance stability for the latter. We develop a semiclassical theory to qualitatively explain this phenomenon, and also provide an understanding based on the random matrix theory through analyzing the local density of states in the dot region and the energy level statistics in the corresponding closed system. Our finding strongly advocates the use of chaotic geometry in quantum dot structures, which is consistent with previous results on smooth conductance fluctuations in classically chaotic systems. In fact, we generally believe that classical chaos has the benefit of bringing in greater stability for quantum devices.

Due to the recent interest in two-dimensional Dirac materials [28], we choose to study quantum dot systems made of graphene [29–35]. There were previous experimental [36–38] and theoretical [39] studies of universal conductance fluctuations in graphene systems. Theoretically and computationally, the effects of disorders were also studied [40–44]. In general, investigating the role of classical chaos in such systems belongs to the emergent field of *relativistic quantum chaos* [45–52].

In Sec. II, we describe our graphene quantum dot systems and the computational method. In Sec. III, we present results

of the average conductance versus the impurity strength and contrast the cases of classically chaotic and integrable dot systems. In Sec. IV, we derive a semiclassical theory to explain, qualitatively, the numerical finding that the chaotic dot exhibits a pronouncedly slower decrease in the average conductance with the impurity strength. In Sec. V, we develop an understanding based on the random matrix theory. In Sec. VI, we present conclusions.

II. MODEL AND COMPUTATIONAL METHOD

Quantum-dot structure with distinct classical dynamics. In order to investigate the effects of classical dynamics on the conductance of the device in the presence of random impurities, we use the tight-binding approximation and the Landauer formalism [53] in combination with the standard Green's function (GF) method [54], which enables a systematic calculation of the conductances for quantum dots of arbitrary geometry. To be concrete, we choose two standard geometrical shapes for the junction region of the dot structure: one of the stadium shape with chaotic dynamics in the classical limit, and another of the rectangular shape with classical integrable dynamics, as shown in Figs. 1(a) and 1(b), respectively. In each case there are random impurities in the dot region. For simplicity, we assume that, in both devices, the semi-infinite leads that are connected to the dot region are made up of perfect ribbons without any disorder.

Hamiltonian. The tight-binding Hamiltonian of the graphene quantum dot system is

$$H = \sum_{\langle i,j \rangle} -t_{ij}(c_i^\dagger c_j + \text{H.c.}) + \sum_i V_i c_i^\dagger c_i, \tag{1}$$

where $t_{ij} = t$ is the electronic hopping energy between two nearest neighboring sites in the lattice, $\langle i,j \rangle$ signifies that the summation is with respect to all nearest-neighbor pairs, and $c_i^\dagger$ and c_i are the creation and annihilation operators at the ith site, respectively. The last term in Eq. (1) describes the effects of impurities of strength V_i on the ith site, where V_i is uniformly distributed in the range $[-W/2, W/2]$, with W being the overall impurity strength.

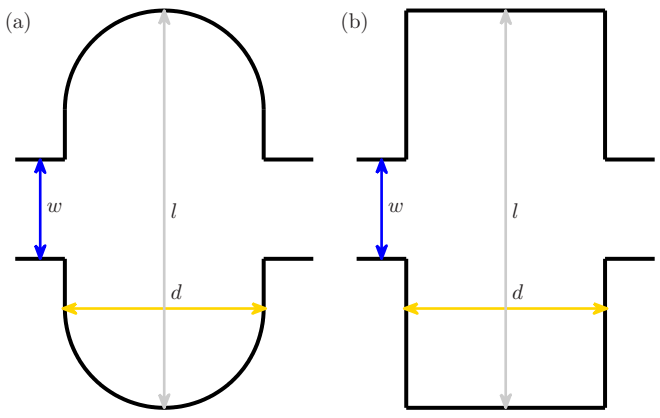

FIG. 1. (Color online) Geometrical dimensions of the quantum dots. (a) Stadium with classical chaotic dynamics and (b) rectangle with classical integrable dynamics.

Green's function formalism. We use the standard Green's function (GF) formalism [54] to calculate the conductance of the quantum-dot system. We calculate the surface retarded Green's functions of the leads and their self-energy functions [55,56]: $\Sigma_{L_\alpha}(E)$, where $\alpha = 1,2$ denote the left and right leads, respectively. The GF of the device can be obtained through

$$G_D(E) = \left[EI - H - \Sigma_{L_1}(E) - \Sigma_{L_2}(E)\right]^{-1}. \tag{2}$$

The quantum transmission of the system is given by $T_{\alpha\beta}(E) = \text{Tr}[\Gamma_{L_\alpha} G_D \Gamma_{L_\beta} G_D^\dagger]$, where $\Gamma_{L_\alpha} = i[\Sigma_{L_\alpha} - \Sigma_{L_\alpha}^\dagger]$ and the subscript $\alpha\beta$ indicates that the transmission is from the βth lead to the αth lead. The conductance can be obtained by the classic Landauer formula:

$$G_{\alpha\beta}(E) = \frac{2e^2}{h} T_{\alpha\beta}(E). \tag{3}$$

The local density of states (LDOS) at the ith site can be obtained as $n_i = -(1/\pi)\text{Im}[G_D(i,i)]$, where $G_D(i,i)$ is the diagonal matrix element of the Green's function at the ith site. The local current element within the linear response regime is given by [57]

$$I_{i\to j}(E_f) = \frac{4e}{\hbar}\text{Im}\left[H_{ij} G_{ji}^n(E_f)\right], \tag{4}$$

where $G_{ji}^n(E_f)$ is the (j,i)th element of the matrix

$$G^n(E_f) = G_D^r(E_f)\left[\Gamma_{L_1} f\left(\mu_{L_1}\right) + \Gamma_{L_2} f\left(\mu_{L_2}\right)\right] G_D^a(E_f),$$

with G_D^r and G_D^a being the retarded and advanced Green's functions, respectively. Here we assume zero temperature so that the Fermi distribution $f(\mu_{L_{1(2)}})$ is a step function. The quantity $\mu_{L_{1(2)}}$ is the chemical potential of the left (right) lead. To ensure linear response, the chemical potentials of both sides are chosen to be close to the Fermi energy of the device. To be concrete we use a slightly higher potential in the left lead than the right lead.

To obtain statistically reliable results for quantum transmission (conductance), for each fixed Fermi energy and impurity strength, we average the conductance using 1000 random realizations of the impurity configuration, making the computation quite demanding. To be feasible, we simulate relatively small devices, with the following geometric parameters: lead width $w \approx 36.92$ Å and 15.62 Å, device width $d \approx 78.7$ Å, and device length $l \approx 151.94$ Å, as shown in Fig. 1. The areas of the stadium and rectangular devices are approximately equal. In order to speed up the computation, we use the recursive Green's function (RGF) method to calculate the conductance by dividing the device into many small layers and calculating the Green's function of each layer under the self energies of all other layers and leads. This way, we replace the inverse of a large matrix by the inverses of many small matrices, leading to a remarkable improvement in the computational efficiency.

In our computations, for the integrable device, the top and bottom boundaries have the zigzag orientation. The chaotic dot shape is cut from the rectangular device with the same boundary orientation. While the orientation of the graphene lattice, i.e., zigzag or armchair, can affect the band structure and the conductance, the lattice orientation is unimportant in our setting because of the random impurities. A previous

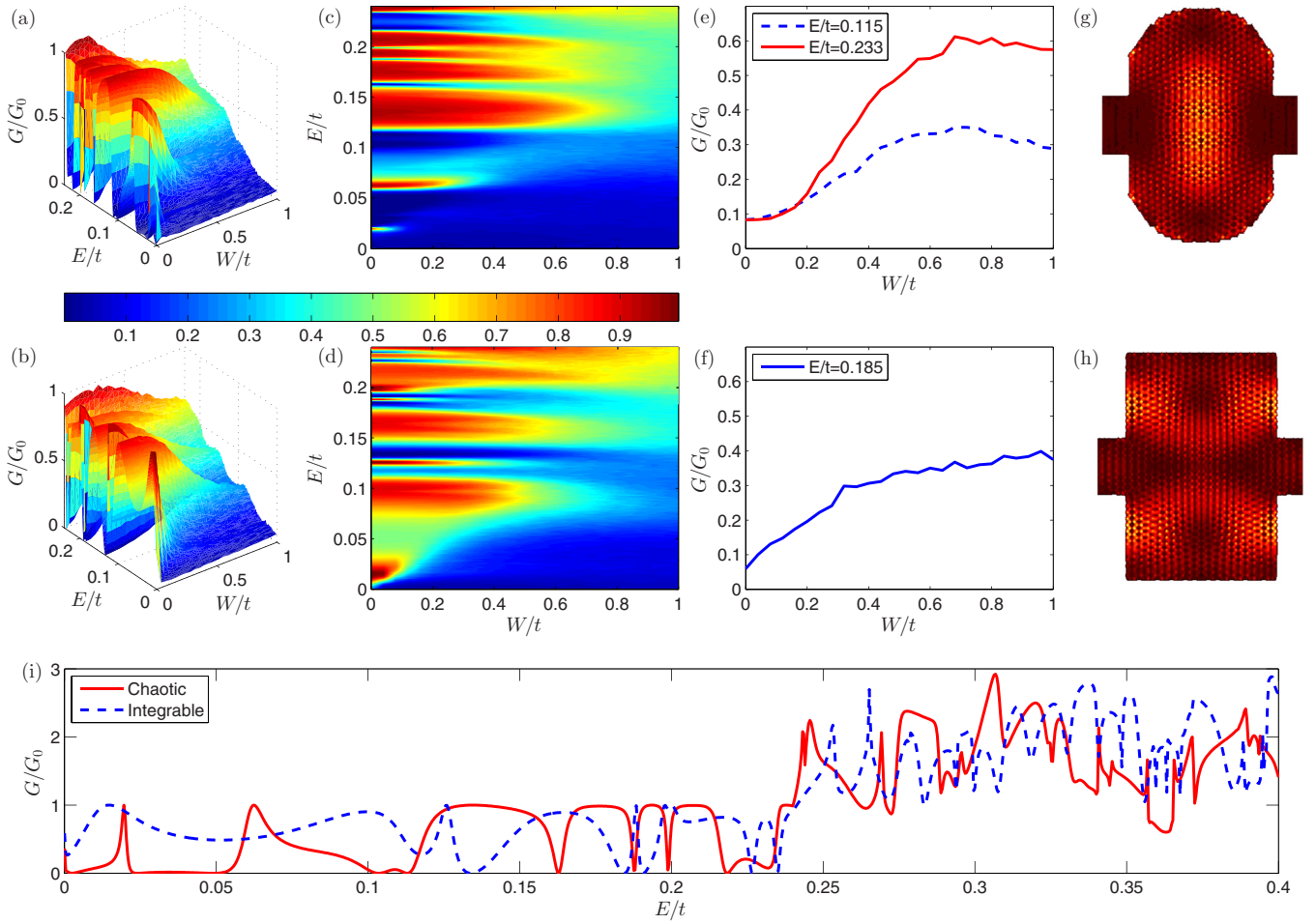

FIG. 2. (Color online) Dependence of the average conductance on the Fermi energy and impurity strength. (a),(b) Three-dimensional plot of the conductance vs the Fermi energy and the impurity strength for classically chaotic and integrable dots, respectively. (c),(d) The corresponding contour plots. (e) Two cases of resonancelike phenomenon for the chaotic geometry for $E/t \approx 0.115$ (red solid line) and 0.233 (blue dashed line). (f) Conductance resonance for the integrable geometry for $E/t \approx 0.185$. (g),(h) Examples of pointer states in absence of any random impurity for the chaotic and integrable cases, respectively. The device structural parameters are lead width $w \approx 36.92$ Å, dot width $d \approx 78.7$ Å, and dot length $l \approx 151.94$ Å. (i) Conductances vs the Fermi energy of the chaotic (red solid line) and integrable (blue dashed line) devices without impurities. For both devices, the width of the first transmission mode is about $0.24t$. The results are in units of $G_0 = 2e^2/h$.

work showed that, for a graphene nanoribbon, although the effect of orientation can be quite significant, when strong short-range impurities are present there is little difference in the average conductances associated with the zigzag and armchair orientations [58]. For the case of weak short-range impurities, the differences between these two orientations can also be neglected for nanoscale devices. The geometrical shapes of the graphene systems in our study are more complicated than nanoribbons. For example, for a chaotic dot structure, different segments of the boundary can have different lattice orientations. The lattice orientation thus will have little effect on our results.

III. RESULTS

The typical behaviors of the ensemble-average conductance versus the Fermi energy and the impurity strength are shown in Figs. 2(a) and 2(b), for classically chaotic and integrable geometries, respectively. The corresponding contour plots are shown in Figs. 2(c) and 2(d). For fixed energy values, two types of behaviors arise in the variation of the conductance with the impurity strength: (1) the conductance increases first as the impurities become stronger, reaches a maximum, and then decreases, and (2) the conductance decreases monotonically with the impurity strength. The first case is somewhat counterintuitive, as exemplified in Fig. 2(e) for $E/t \approx 0.115, 0.233$ for the chaotic dot and in Fig. 2(f) for $E/t \approx 0.185$ for the integrable geometry. This resonancelike phenomenon was reported previously [44], where the initial conductance enhancement can be attributed to the breakdown of the edge states in graphene by weak impurities. However, for strong impurity the quantum states are localized, reducing the conductance. Here we find, for all cases where such a resonance phenomenon occurs, the conductance value for the zero impurity case must be close to zero. That is, when the system is free of any random impurity, the system is already in some pointer state, providing a "room" for impurity to break the state and consequently to enhance the conductance. Two examples of the pointer states in the absence of any impurity are shown in Figs. 2(g) and 2(h), respectively, for

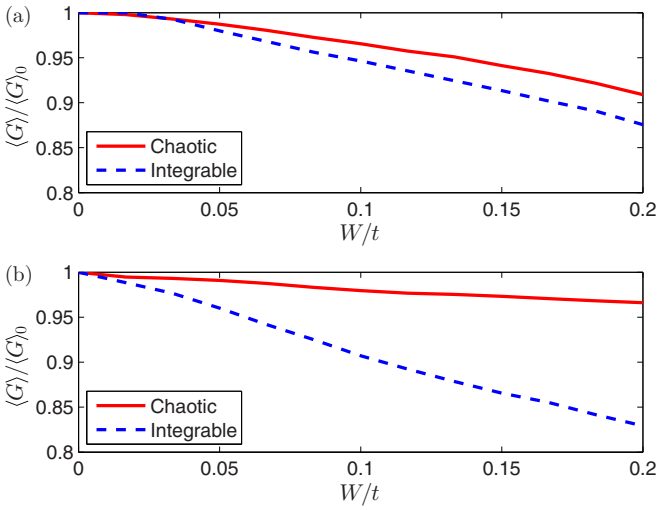

FIG. 3. (Color online) Effect of lead width on conductance stability. Average conductance over the energy range of the first transmission mode of the lead vs the impurity strength for (a) lead width $w \approx 36.92$ Å and (b) lead width $w \approx 15.62$ Å. The blue (dashed) and red (solid) curves correspond to classically integrable and chaotic dot structures, respectively. We use $\langle G\rangle_0 = \langle G\rangle(W = 0)$ to normalize the average conductance. Note that $\langle G\rangle_0$ should be distinguished from the natural conductance unit G_0.

the chaotic and integrable dots. If, for certain Fermi energy, in the absence of any impurity the quantum state is not a pointer state so that the conductance has a relatively large value, introducing impurities into the system can only serve to reduce the conductance, ruling out any possible increase in the conductance and consequently resonance.

To address the conductance stability and to better understand the effect of the interplay between random impurities and classical dynamics on conductance, we examine the average conductance as a function of the impurity strength. In particular, for a fixed value of the impurity strength, we average the conductance over the Fermi energy in the range defined by the first transmission mode of the graphene device, which is about $0.24t$ in our cases. For the dot parameters as in Fig. 2, the normalized average conductance behaviors are shown in Fig. 3(a), where the blue (dashed) and red (solid) curves correspond to the integrable and chaotic cases, respectively. We see that, as the impurity strength is increased, the average (or overall) conductance decreases monotonically for both cases. However, for the chaotic dot, the slope of the decreasing trend is smaller than that for the integrable dot. This behavior persists with respect to variations in the device parameters. For example, Fig. 3(b) shows a case with the lead width reduced to $w \approx 15.62$ Å. These results indicate that the conductance of the chaotic dot is more "stable" with respect to variations in the strength of random impurities.

IV. SEMICLASSICAL UNDERSTANDING OF THE INTERPLAY BETWEEN RANDOM IMPURITIES AND CLASSICAL DYNAMICS

Our main numerical result is that classical chaos makes the average conductance of the quantum dot less sensitive to random impurities than integrable dynamics. In particular, as demonstrated in Fig. 3, the derivative of the average conductance with respect to the impurity strength, $d\langle G\rangle(W)/dW$, is negative but its absolute value is small for the chaotic dot and relatively large for the integrable dot. It is possible to obtain a qualitative understanding of the behavior of the derivatives using a semiclassical argument.

For a general open Hamiltonian system, the elements of the quantum S matrix can be expressed via classical quantities through the Miller [27] formula:

$$S_{\mu\nu}(E) = \sum_s \left[P^{(s)}_{\nu\to\mu}(E)\right]^{1/2} \exp\left[\frac{i}{\hbar}\Phi^{(s)}(E) - \frac{i\pi}{2}\xi^{(s)}\right], \quad (5)$$

where μ and ν denote quantum states, "(s)" denotes a classical path, $P^{(s)}_{\nu\to\mu}(E)$ is the classical transition probability from state ν to state μ along (s), $\xi^{(s)}$ is the Maslov index, and the sum is over all the classical paths connecting states ν and μ. Let (I_ν,θ_ν) and (I_μ,θ_μ) be the action-angle variables associated with states ν and μ, respectively. The classical transition probability is given by [27] $P^{(s)}_{\nu\to\mu}(E) = (1/2\pi)|\partial I_\mu/\partial\theta_\nu|^{-1}_s$. In the study of quantum chaotic scattering, a seminal result [8,9] is that the energy autocorrelation function of an S-matrix element, defined as $C_{\mu\nu}(\varepsilon) \equiv \langle S^*_{\mu\nu}(E)S_{\mu\nu}(E+\varepsilon)\rangle$, can be obtained through Eq. (5) as a Fourier transform of the classical particle decay probability:

$$C_{\mu\nu}(\varepsilon) = \int dt\,\langle P_{\mu\nu}(E,t)\rangle_E \exp(i\varepsilon t/\hbar), \quad (6)$$

where t is the time that a classical particle dwells in the scattering (dot) region, $\langle P_{\mu\nu}(E,t)\rangle$ is the classical probability that a $\nu\to\mu$ transition occurs with the corresponding delay time in the interval $[t,t+dt]$, and the average $\langle\cdot\rangle_E$ is over a classically small but quantum mechanically large energy interval. For our single-mode quantum dot system in the presence of random impurity of strength W, we have $\mu = \nu = 1$ so we write $\langle P(t;E,W)\rangle$, which is the probability density for a particle to have dwelling time in the range $[t,t+dt]$. The average conductance is given by

$$\langle G\rangle(W) \sim C_{\mu\nu}(0) \sim \left|\lim_{\varepsilon\to 0}\int dt\,\langle P_{\mu\nu}(t;E,W)\rangle_E \exp(i\varepsilon t/\hbar)\right|. \quad (7)$$

For a chaotic dot, regardless of the presence of random impurities, the particle decay law is exponential: $\langle P(t;E,W)\rangle_E \sim e^{-t/\tau(W)}$, where $\tau(W)$ is the average lifetime that a classical particle stays in the dot region. Due to classical chaos, the scattering is random in the dot region. If there are no stable periodic orbits (as in the stadium dot), scattering is already sufficiently random so that the introduction of impurities will enhance the randomness only incrementally, causing insignificant decrease in the average lifetime. It is thus reasonable to assume little dependence of the average lifetime τ on W: $d\tau(W)/dW \lesssim 0$. Numerically it may be nontrivial to calculate the particle decay law in the presence of impurities—see Appendix for a detailed description of our procedure and numerical parameters.

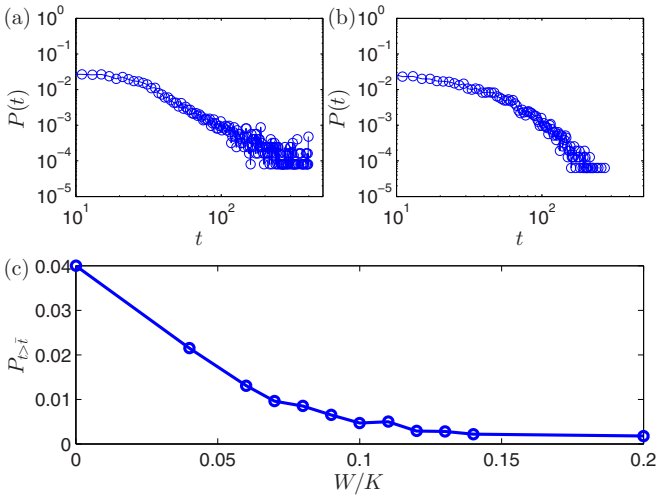

FIG. 4. (Color online) Classical scattering dynamics for the integrable quantum dot. (a),(b) For the integrable dot, particle dwelling time distribution without and with random impurities, i.e., $W/K = 0.0$ and $W/K = 0.2$ (where K is the kinetic energy of the classical particle), respectively, on a double logarithmic scale. We see that the former exhibits an algebraically decaying behavior and the latter shows a mixture of algebraically and exponentially decaying behavior. (c) The probability of having particles with long dwelling time vs the impurity strength. A detailed description of the numerical procedure and the parameters is given in the Appendix.

Substituting the exponential decay law into Eq. (7), we obtain $\langle G\rangle(W) \sim \tau(W)$ so that

$$d\langle G\rangle(W)/dW \lesssim 0, \tag{8}$$

which explains the slow decrease in the average conductance with the impurity strength for the chaotic dot.

For an integrable dot without random impurities, the classical particle decay is algebraic, as shown in Fig. 4(a). When random impurities are present, the decay law is a mixture of algebraic and exponential behaviors, as shown in Fig. 4(b). Especially, as the impurity strength is increased, random scattering becomes progressively significant so that the "weight" of the exponential decay gradually dominates. A plausible mathematical expression for the decay law is

$$\langle P(t;E,W)\rangle_E \sim \begin{cases} at^{-\alpha_c}, & t_0 < t < t_c, \\ b\,\exp\left[-(t-t_c)/\beta_c\right], & t > t_c, \end{cases} \tag{9}$$

where a, b, α_c, and β_c are all positive constants and t_c is the "crossover" time, above which there is a transition from algebraic to exponential decay as t is increased. The relative magnitudes of the constants can be estimated, as follows. The value of the algebraic decay exponent α_c is typically between 1 and 2 for two degrees of freedom Hamiltonian systems [59–62]. For relatively weak impurities, the crossover from algebraic to exponential behaviors occurs at some large time t_c, which should be much larger than the exponential decay lifetime β_c because the particles tend to leave the scattering region fast once the algebraic behavior is over and random scattering from the impurities dominates. It is thus reasonable to assume $\beta_c \ll t_c$. At the crossover time t_c, we have $b \approx at_c^{-\alpha_c}$. Since the decay is relatively slow for $t < t_c$, the probability for particle to stay in the dot region can be appreciable for $t = t_c$. We thus have $b \approx at_c^{-\alpha_c} \lesssim 1$.

As the impurity strength W is increased, we expect t_c to decrease. With the aid of numerical simulation, we can reason that $dt_c(W)/dW < 0$ must hold and $|dt_c(W)/dW|$ is far from being negligible. Specifically, we numerically calculate, for a set of systematically varying values of W, the classical probability $P_{t>\bar{t}}(W)$ that a particle stays in the scattering region for $t > \bar{t} > t_c$. As W is increased, we expect $P_{t>\bar{t}}(W)$ to decrease. A typical example is shown in Fig. 4(c), where we observe that $P_{t>\bar{t}}(W)$ decreases rapidly with W. Write $P_{t>\bar{t}}(W) = f(W) > 0$, the probability that a particle has a dwell time longer than $\bar{t}$, where $df(W)/dW < 0$ but $|df(W)/dW|$ is large [$f(W)$ can be obtained numerically]. Utilizing Eq. (9), we have

$$\begin{aligned} f(W) &= \int_{\bar{t}}^{\infty} b\,\exp\{-[t - t_c(W)]/\beta_c\}dt \\ &= a\beta_c[t_c(W)]^{-\alpha_c}\exp\{-[\bar{t} - t_c(W)]/\beta_c\}, \end{aligned}$$

which gives

$$\frac{dt_c(W)}{dW} = \frac{df(W)/dW}{f(W)}\frac{1}{1/\beta_c - \alpha_c/t_c(W)}.$$

Since $\alpha_c \sim 1$ and $\beta_c \ll t_c(W)$, we see that the sign of the derivative $dt_c(W)/dW$ is the same as the sign of $df(W)/dW$, which is negative. In addition, we have $|dt_c(W)/dW| \approx |df(W)/dW \cdot \beta_c/f(W)|$.

Substituting Eq. (9) into Eq. (7), we obtain the average conductance for the integrable dot system in the presence of impurities as

$$\langle G\rangle(W) \sim a\frac{[t_c(W)]^{1-\alpha_c}}{1-\alpha_c} - a\frac{[t_0]^{1-\alpha_c}}{1-\alpha_c} + a\beta_c[t_c(W)]^{-\alpha_c},$$

which gives

$$\begin{aligned} \frac{d\langle G\rangle(W)}{dW} &\sim a[t_c(W)]^{-\alpha_c}\left[1 - \frac{\alpha_c\beta_c}{t_c(W)}\right]\frac{dt_c(W)}{dW} \\ &\sim e^{[\bar{t}-t_c(W)]/\beta_c}\left[1 - \frac{\alpha_c\beta_c}{t_c(W)}\right]\frac{df(W)}{dW} \\ &\equiv A(W)\frac{dt_c(W)}{dW}. \end{aligned} \tag{10}$$

Since $\bar{t} > t_c$, $\alpha_c \sim 1$, and $\beta_c \ll t_c(W)$, the factor $A(W)$ in Eq. (10) is positive and not negligibly small. We thus have

$$\frac{d\langle G\rangle(W)}{dW} < 0 \quad \text{and} \quad \left|\frac{d\langle G\rangle(W)}{dW}\right| \sim \left|\frac{dt_c(W)}{dW}\right| \quad \text{(large)}. \tag{11}$$

Relations (8) and (11), for chaotic and integrable quantum dots, respectively, represent a semiclassical understanding of the results in Fig. 3.

V. UNDERSTANDING BASED ON RANDOM MATRIX THEORY

In situations where a quantum dot exhibits fully developed chaos in the classical limit and/or has stationary random impurities, electrons injected from the leads will scatter elastically from the dot boundaries and/or from the random

impurities. If the mean free path of the electron is much shorter than the size of the dot, i.e., $l_{MFP} \ll d$, the transport is diffusive and the time of electrons dwelling in the dot region satisfies $\tau_{\rm dwell} \gg \tau_{\rm erg}$, where $\tau_{\rm erg}$ is the time required for a typical classical trajectory to explore the phase space in an ergodic manner [63–65], due to chaos and/or random scattering. The scattering matrix is effectively random, which can be described through the Wigner-Dyson random-matrix theory (RMT). In RMT, the transmission coefficient distribution for a single mode is given by [66–68]

$$P(T) = \frac{\beta_T}{2} T^{\beta_T/2-1}, \tag{12}$$

where the range of the transmission is $0 \leqslant T \leqslant 1$ and $\beta_T = 1$ if there is no magnetic field present, and $P(T)$ approaches a circular distribution. A previous work [66] demonstrated that the distribution is highly non-Gaussian, especially for systems where the number of transmission modes is less than three. However, for leads that permit many modes, the transmission distribution approaches Gaussian.

For simplicity, we consider a single-mode quantum-dot system that is fully chaotic in the classical limit. Integrating Eq. (12) for transmission in the range [0,1], we obtain the average conductance as

$$\langle G\rangle_{\rm single}/G_0 = \langle T\rangle = \frac{\beta_T}{\beta_T+2} = \frac{1}{2} + \frac{\beta_T-2}{2\beta_T+4}, \tag{13}$$

where the first term 1/2 is the "classical" conductance for the chaotic cavity with the physical meaning that a classical particle has equal probability to transmit through and to reflect back from the dot region. The second term is the correction due to quantum interference, also known as the weak localization effect [63] for $\beta_T = 1$, which vanishes when the time-reversal symmetry is broken ($\beta_T = 2$), e.g., when a perpendicular magnetic field is present. If there is spin-orbit coupling ($\beta_T = 4$), the second term becomes positive and the transmission is enhanced, a phenomenon known as weak antilocalization.

Figure 5(a) shows the numerically obtained statistics of the transmission for the chaotic (red circle) and integrable (blue square) graphene quantum-dot systems. In order to make the effects of chaotic geometry more pronounced, we consider relatively large devices, each having over 10 000 atoms, and choose narrow waveguide width so that the coupling between the leads and the dot region is relatively weak. For the chaotic dot system, the transmission distribution agrees well with the prediction in Eq. (12), especially in the low-transmission regime, as shown in Fig. 5(a). The corresponding average conductance is $\langle G\rangle_{\rm stad}/G_0 = 0.3457$, which is approximately equal to the theoretical prediction $\langle G\rangle_{\beta_T=1}/G_0 = 1/3$. For the integrable dot system, the transmission distribution deviates from that for the chaotic case in the low- and high-transmission regimes. However, in the intermediate-transmission regime (e.g., $0.2 < T < 0.8$), there is no apparent difference between the two cases, as shown in Fig. 5(a). The mean conductance of the integrable dot system is $\langle G\rangle_{\rm rect}/G_0 = 0.4544$, which is larger than that for the chaotic dot system. From Fig. 5(a), we see that, for the integrable dot system, there are fewer (more) counts of low (high) transmission values as compared with the chaotic dot system. The differences can be seen more clearly in Fig. 5(b). The reason is that the integrable dot system has a high degree of geometric symmetry, for which quantum pointer states [56,69] can form, leading to Fano resonances [20–24] in the transmission (e.g., as a function of the Fermi energy). The resonances contribute to more counts of much higher-than-average transmission values. Symmetry breaking can lead to chaos. For a chaotic dot, the probability for pronounced pointer states to form is significantly lower than that for an integrable dot system so that sharp Fano resonances are much less likely. In this case, the transmission fluctuations tend to be more smooth, giving rise to few counts of extreme transmission values.

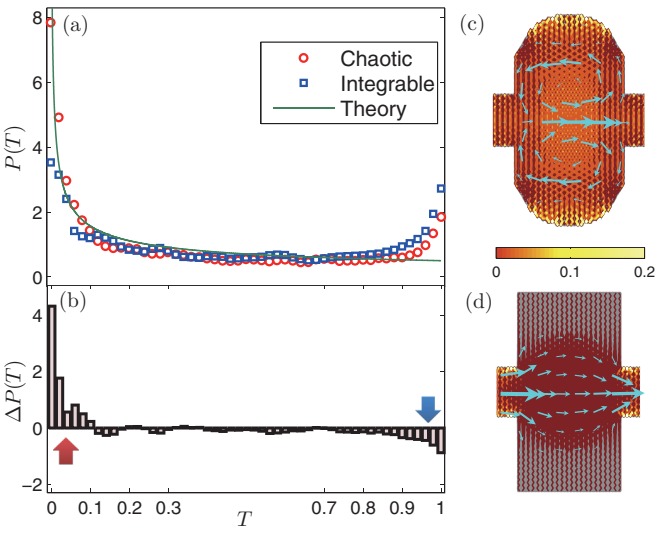

FIG. 5. (Color online) Transport statistics for chaotic and integrable graphene quantum dots. The width of the leads is $w = 6.5a$ with single mode transport in the energy range $0 \leqslant E/t \leqslant 0.796$. For both cases, the ratio of the height and width is $h/d = 1.8$. For the chaotic (integrable) dot system, there are 12014 (13464) atoms in the scattering region. (a) Transmission coefficient distribution $P(T)$ for the chaotic (blue circles) and integrable (red squares) dots. The gray solid curves correspond to the RMT prediction [Eq. (12)]. (b) Differences in the transmission distribution between the two cases. (c),(d) LDS patterns showing the electron distribution in the physical space, where the gray arrows depict the directions of the local currents. The energy values for the chaotic and integrable cases are $E/t = 0.1048$ and $E/t = 0.048$, respectively.

The distribution of transmission $P(T)$ in Fig. 5(a) is different from that of the transmission eigenvalues $\rho(T_n)$ obtained from the fixed-energy transmission coefficient between different modes [70]. A transmission matrix can then be constructed with elements t_{mn} and T_n being the eigenvalue of the matrix $t^\dagger t$ for a fixed Fermi energy, where m and n are mode indices. Since we focus on the single-mode case ($N_{\rm channel} = 1$), the matrix is reduced to a number.

We observe, however, that for the stadium dot system, there are more counts of very high-transmission values than predicted, which can be understood again by resorting to the consideration of symmetry. In particular, the theoretical curve describes the situation of fully developed classical chaos [68] without any geometric symmetry. The chaotic (stadium) dot used in our computation does in fact possess

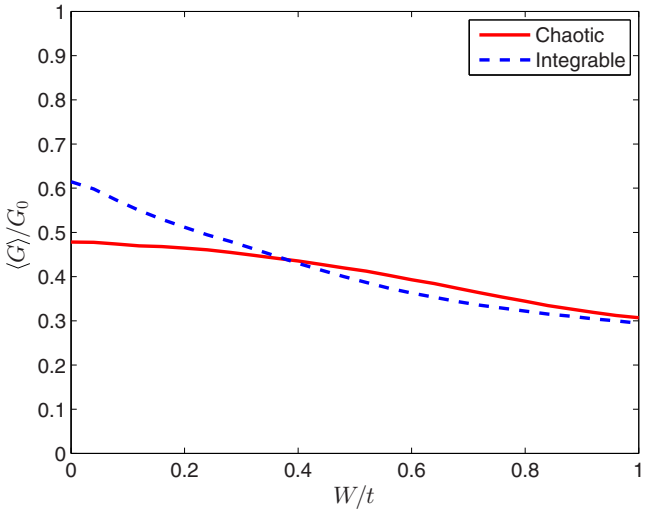

FIG. 6. (Color online) Behaviors of unnormalized conductance. For lead width $w \approx 36.92$ Å, unnormalized average transmission over the energy range of the first transmission mode of the graphene lead vs the impurity strength, for the chaotic (red solid line) and integrable (blue dashed line) dot systems. For sufficiently strong disorder, the difference in the average transmission values for the two cases diminishes.

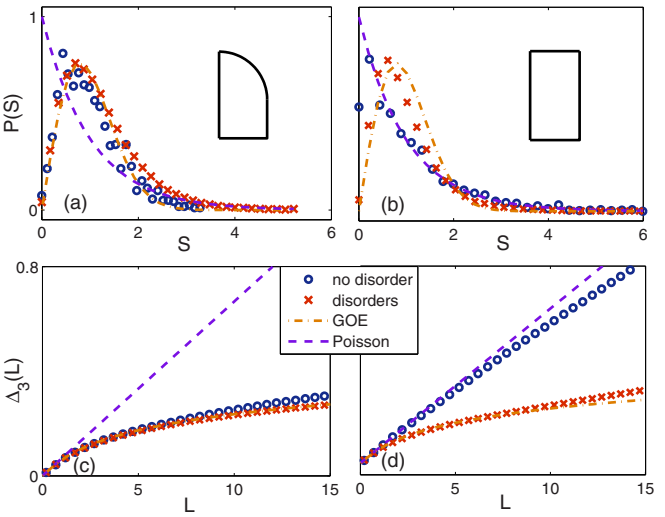

FIG. 7. (Color online) Energy level statistics of chaotic and integrable quantum dots as predicted by the random matrix theory. Level spacing statistics for (a),(c) chaotic and (b),(d) integrable closed billiard systems. The ratio of the height and the width for both geometries in (a),(b) is the same as that of the geometries used to calculate the transmission in Fig. 5. There are 11777 carbon atoms in the unfolded stadium system and 13340 atoms in the rectangular system. In (a),(b), the unfolded level-spacing distributions $P(S)$ are shown, with the corresponding spectral rigidity Δ_3 for energy levels in the range of $0.1 < E_n/t < 1$ shown in (c),(d). The impurity strength is $W = 0.2t$. Each data point is the result of averaging over 100 random impurity configurations.

certain geometry. The finite width of the leads and their symmetric locations on both sides of the device allows ballistic transport channels [71,72] to be bridged, leading to nearly unity maximum transmission.

Figures 5(c) and 5(d) show, for the chaotic and integrable dot systems, respectively, a set of typical patterns of LDOS and local currents. For the integrable system, there are current channels of direct transport through which electrons transmit with little scattering [52,73–75], as indicated by the current direction in Fig. 5(d). In the absence of random impurities, the average transmission value is thus higher for the integrable system. As impurities are introduced into the system, even in the integrable system there are random scatterings. As the impurity strength is increased, the average transmission value decreases. For sufficiently strong impurities, the difference between the chaotic and integrable geometries diminishes, leading to approximately the same average transmission value. An example of this behavior is shown in Fig. 6. Thus, in the same range of variation of the impurity strength, the average transmission for the integrable system needs to decrease by a larger amount, leading to a larger slope of decrease in the average normalized transmission, as exemplified in Fig. 3.

To gain further insights, we investigate the integrable and chaotic dot structures from the angle of energy level-spacing statistics. For the corresponding closed systems (e.g., by making the lead width tend to zero), we can calculate a large number of energy levels. In the absence of any random impurity, the level-spacing distributions for the underlying systems are GOE [Gaussian orthogonal ensemble, $P(S) = (\pi/2)S\,e^{-\pi S^2/4}$] and Poisson [$P(S) = e^{-S}$] for chaotic and integrable geometries [47], respectively, where S stands for the normalized nearest-neighbor level spacing. When there are random impurities and as the impurity strength is increased, we expect the difference in the level spacing statistics for the two cases to diminish. Figures 7(a) and 7(b) show $P(S)$ for the chaotic and integrable dot systems, respectively. In each panel, the blue circles and the red crosses are for the cases where random impurities are absent and present, respectively, where the results are obtained using 100 random impurity configurations. We see that, even in the presence of relatively weak impurities ($W = 0.2t$), the level-spacing statistics of both the chaotic and integrable systems are GOE. This convergence to GOE statistics can be more clearly seen through the spectral rigidity, as shown in Figs. 7(c) and 7(d). These results suggest the equivalent effects of classical chaos and impurities: both generating random scattering in both classical and quantum regimes. For an integrable dot system, there is thus a dramatic change in the underlying quantum scattering as impurity is introduced and its strength is increased: from little to significant random scattering. As a result, the average transmission and other device properties tend to exhibit significant changes. However, for a chaotic dot system, the presence of impurities hardly changes the quantum scattering dynamics. From this perspective, chaotic dot systems possess a higher degree of stability against random impurities than integrable dot systems.

We note that the quantum pointer states are localized states with long lifetimes and less interactions with the environment. They are related to the stable classical periodic orbits and eigenstates of a closed dot [19]. Previous works showed that change in the geometry of the device, e.g., from integrable to chaotic, can lead to a reduction of the number of quantum pointer states [25]. Random impurities can also reduce the

number of quantum pointer states. However, if a strong magnetic field is present, the nature of the classical dynamics and/or random impurities will have less pronounced effects on quantum transport [17,18,74]. One set of the quantum pointer states are associated with the stable orbits within the KAM islands in the classical phase space. The probability that these states can be affected significantly by random disorders is small. The corresponding quantum pointer states can then be quite persistent.

VI. CONCLUSION

The role of classical chaos in suppressing quantum fluctuations has been recognized in the contexts of quantum chaotic scattering [7–9] and transport through quantum dots [25,26] for more than two decades. For integrable or mixed classical dynamics, there are stable periodic orbits in the phase space. The corresponding bounded states typically have little interactions with the leads, giving rise to sharp Fano resonances in the dependence of the conductance on the Fermi energy [21–24,69]. However, fully developed chaos gives rise to strong ergodicity of classical orbits, enabling strong interaction between the quantum states in the scattering regions and in the leads. It is then difficult for long-lived quantum states to form in the dot region, leading to near-zero probability for pointer states and Fano resonance. As a result, conductance fluctuations tend to be much more smooth then those in integrable or mixed quantum dots. In this sense, while chaos usually generates random dynamical behaviors classically, quantum mechanically it can lead to suppressed fluctuations. A similar phenomenon arises in the context of quantum resonant tunneling, both non-relativistically [76,77] and relativistically [49].

This paper deals with the interplay between chaos, random impurities, and quantum behaviors. The main finding is that chaos can be exploited to stabilize quantum behaviors in the presence of impurities, which is consistent with previous works on conductance fluctuations and resonant tunneling. Especially, we focus on the average conductance and ask how it may be affected by random impurities for two cases where the corresponding classical dynamics are chaotic and integrable, respectively. In general, as the impurity strength is increased, the average conductance will decrease, and we find that the decreasing behavior tends to be much less pronounced for the chaotic quantum dot. That is, for a wide range of the impurity strength, the average conductance changes only a little if there is chaos in the classical limit. We develop a physical understanding of this phenomenon using both semiclassical and random-matrix theories. Our work provides a further case where chaos can be advantageous from the standpoint of making stable quantum devices.

ACKNOWLEDGMENTS

We thank H.-Y. Xu for discussions. This work was supported by AFOSR under Grant No. FA9550-15-1-0151.

APPENDIX: CLASSICAL SIMULATION OF SCATTERING DYNAMICS IN THE PRESENCE OF RANDOM IMPURITIES

We simulate the dynamics of the classical particles in the quantum dot system in the presence of impurities that are modeled by Gaussian random potentials, using the standard leap-frog method for numerically solving Hamiltonian systems [78]. The method is able to maintain the time reversibility of the system and conserve the energy during the simulation. The Hamiltonian of the classical system can be written as

$$H_{LF} = K(v_x, v_y) + U(x, y),$$

where

$$K(v_x, v_y) = \frac{1}{2} m\left(v_x^2 + v_y^2\right),$$

$$U(x, y) = \sum_i V_i' \exp\left[-\frac{(x - x_i)^2 + (y - y_i)^2}{2\sigma_i^2}\right],$$

x_i and y_i are the coordinates of the center of the ith Gaussian potential, V_i' is its strength uniformly distributed within $[-W/2, W/2]$, and σ_i characterizes the range of the ith potential.

In our simulations, we use the width of the device to rescale the length. For example, if in the quantum simulations there are about 4000 atoms in the dot, classically we distribute $N' = 4000$ random Gaussian potentials throughout the scattering region. We set $d' = 1.0$ and $l' = 1.8$. We assume the range of each potential to be the same and $\sigma_i = \sigma$ can be approximately calculated from $\sqrt{d'l'/(2\pi N')} = 0.0085$. Without loss of generality, we use $\sigma = 10^{-3}$ in our simulations. We keep the kinetic energy K of the particles to be the same for all cases and change the ratio of W/K to simulate the particle dynamics in the presence of random impurities of systematically varying strength. In particular, in the interior of the dot region, the classical evolution is obtained by solving the Hamilton's equations of motion using the leap-frog method. The boundaries are assumed to be hard so that at any boundary point of collision the particle trajectory is simply reflected.

[1] P. A. Lee and A. D. Stone, Phys. Rev. Lett. **55**, 1622 (1985).
[2] C. P. Umbach, S. Washburn, R. B. Laibowitz, and R. A. Webb, Phys. Rev. B **30**, 4048 (1984).
[3] R. A. Webb, S. Washburn, C. P. Umbach, and R. B. Laibowitz, Phys. Rev. Lett. **54**, 2696 (1985).
[4] A. D. Stone, Phys. Rev. Lett. **54**, 2692 (1985).
[5] R. A. Jalabert, H. U. Baranger, and A. D. Stone, Phys. Rev. Lett. **65**, 2442 (1990).
[6] H.-J. Stöckmann, *Quantum Chaos: An Introduction* (Cambridge University Press, New York, 1999).
[7] R. Blümel and U. Smilansky, Phys. Rev. Lett. **60**, 477 (1988).
[8] R. Blümel and U. Smilansky, Physica D **36**, 111 (1989).
[9] Y.-C. Lai, R. Blümel, E. Ott, and C. Grebogi, Phys. Rev. Lett. **68**, 3491 (1992).
[10] C. M. Marcus, A. J. Rimberg, R. M. Westervelt, P. F. Hopkins, and A. C. Gossard, Phys. Rev. Lett. **69**, 506 (1992).

[11] R. Ketzmerick, Phys. Rev. B **54**, 10841 (1996).
[12] A. S. Sachrajda, R. Ketzmerick, C. Gould, Y. Feng, P. J. Kelly, A. Delage, and Z. Wasilewski, Phys. Rev. Lett. **80**, 1948 (1998).
[13] B. Huckestein, R. Ketzmerick, and C. H. Lewenkopf, Phys. Rev. Lett. **84**, 5504 (2000).
[14] G. Casati, I. Guarneri, and G. Maspero, Phys. Rev. Lett. **84**, 63 (2000).
[15] A. P. S. de Moura, Y.-C. Lai., R. Akis, J. P. Bird, and D. K. Ferry, Phys. Rev. Lett. **88**, 236804 (2002).
[16] R. Crook, C. G. Smith, A. C. Graham, I. Farrer, H. E. Beere, and D. A. Ritchie, Phys. Rev. Lett. **91**, 246803 (2003).
[17] D. K. Ferry, A. M. Burke, R. Akis, R. Brunner, T. E. Day, R. Meisels, F. Kuchar, J. P. Bird, and B. R. Bennett, Semicond. Sci. Technol. **26**, 043001 (2011).
[18] R. Brunner, D. K. Ferry, R. Akis, R. Meisels, F. Kuchar, A. M. Burke, and J. P. Bird, J. Phys.: Condens. Matter **24**, 343202 (2012).
[19] D. K. Ferry, L. Huang, R. Yang, Y.-C. Lai, and R. Akis, J. Phys.: Conf. Ser. **220**, 012015 (2010).
[20] U. Fano, Phys. Rev. **124**, 1866 (1961).
[21] A. E. Miroshnichenko, S. Flach, and Y. S. Kivshar, Rev. Mod. Phys. **82**, 2257 (2010).
[22] L. Huang, Y.-C. Lai, H.-G. Luo, and C. Grebogi, AIP Adv. **5**, 017137 (2015).
[23] Y. Yoon, M.-G. Kang, T. Morimoto, M. Kida, N. Aoki, J. L. Reno, Y. Ochiai, L. Mourokh, J. Fransson, and J. P. Bird, Phys. Rev. X **2**, 021003 (2012).
[24] J. Fransson, M.-G. Kang, Y. Yoon, S. Xiao, Y. Ochiai, J. L. Reno, N. Aoki, and J. P. Bird, Nano Lett. **14**, 788 (2014).
[25] R. Yang, L. Huang, Y.-C. Lai, and L. M. Pecora, Appl. Phys. Lett. **100**, 093105 (2012).
[26] R. Yang, L. Huang, Y.-C. Lai, C. Grebogi, and L. M. Pecora, Chaos **23**, 013125 (2013).
[27] W. H. Miller, Adv. Chem. Phys. **25**, 69 (1974).
[28] A. H. C. Neto and K. Novoselov, Mater. Exp. **1**, 10 (2011).
[29] K. S. Novoselov, A. K. Geim, S. V. Morozov, D. Jiang, Y. Zhang, S. V. Dubonos, I. V. Grigorieva, and A. A. Firsov, Science **306**, 666 (2004).
[30] C. Berger, Z. M. Song, T. B. Li, X. B. Li, A. Y. Ogbazghi, R. F. Z. T. Dai, A. N. Marchenkov, E. H. Conrad, P. N. First, and W. A. de Heer, J. Phys. Chem. B **108**, 19912 (2004).
[31] K. S. Novoselov, A. K. Geim, S. V. Morozov, D. Jiang, M. I. Katsnelson, I. V. Grigorieva, S. V. Dubonos, and A. A. Firsov, Nature (London) **438**, 197 (2005).
[32] Y. B. Zhang, Y. W. Tan, H. L. Stormer, and P. Kim, Nature (London) **438**, 201 (2005).
[33] A. H. Castro Neto, F. Guinea, N. M. R. Peres, K. S. Novoselov, and A. K. Geim, Rev. Mod. Phys. **81**, 109 (2009).
[34] N. M. R. Peres, Rev. Mod. Phys. **82**, 2673 (2010).
[35] S. D. Sarma, S. Adam, E. H. Hwang, and E. Rossi, Rev. Mod. Phys. **83**, 407 (2011).
[36] S. V. Morozov, K. S. Novoselov, M. I. Katsnelson, F. Schedin, L. A. Ponomarenko, D. Jiang, and A. K. Geim, Phys. Rev. Lett. **97**, 016801 (2006).
[37] C. Berger, Z. Song, X. Li, X. Wu, N. Brown, C. Naud, D. Mayou, T. Li, J. Hass, A. N. Marchenkov, E. H. Conrad, P. N. First, and W. A. de Heer, Science **312**, 1191 (2006).
[38] H. B. Heersche, P. Jarillo-Herrero, J. B. Oostinga, L. M. K. Vandersypen, and A. F. Morpurgo, Nature (London) **446**, 56 (2007).
[39] D. W. Horsell, A. K. Savchenko, F. V. Tikhonenko, K. Kechedzhi, and I. V. Lerner, Solid State Commun. **149**, 1041 (2009).
[40] A. Rycerz, J. Tworzydło, and C. Beenakker, EPL **79**, 57003 (2007).
[41] W. Long, Q.-f. Sun, and J. Wang, Phys. Rev. Lett. **101**, 166806 (2008).
[42] I. Amanatidis and S. N. Evangelou, Phys. Rev. B **79**, 205420 (2009).
[43] R. Ma, L. Sheng, R. Shen, M. Liu, and D. N. Sheng, Phys. Rev. B **80**, 205101 (2009).
[44] L.-L. Jiang, L. Huang, R. Yang, and Y.-C. Lai, Appl. Phys. Lett. **96**, 262114 (2010).
[45] M. V. Berry and R. J. Mondragon, Proc. R. Soc. London, Ser. A: Math. Phys. Eng. Sci. **412**, 53 (1987).
[46] L. Huang, Y.-C. Lai, D. K. Ferry, S. M. Goodnick, and R. Akis, Phys. Rev. Lett. **103**, 054101 (2009).
[47] L. Huang, Y.-C. Lai, and C. Grebogi, Phys. Rev. E **81**, 055203 (2010).
[48] R. Yang, L. Huang, Y.-C. Lai, and C. Grebogi, EPL **94**, 40004 (2011).
[49] X. Ni, L. Huang, Y.-C. Lai, and L. M. Pecora, EPL **98**, 50007 (2012).
[50] X. Ni, L. Huang, Y.-C. Lai, and C. Grebogi, Phys. Rev. E **86**, 016702 (2012).
[51] H. Y. Xu, L. Huang, Y.-C. Lai, and C. Grebogi, Phys. Rev. Lett. **110**, 064102 (2013).
[52] L. Ying, G. Wang, L. Huang, and Y.-C. Lai, Phys. Rev. B **90**, 224301 (2014).
[53] R. Landauer, Philos. Mag. **21**, 863 (1970).
[54] S. Datta, *Electronic Transport in Mesoscopic Systems* (Cambridge University Press, Cambridge, UK, 1997).
[55] T. C. Li and S.-P. Lu, Phys. Rev. B **77**, 085408 (2008).
[56] L. Huang, Y.-C. Lai, D. K. Ferry, R. Akis, and S. M. Goodnick, J. Phys.: Condens. Matter **21**, 344203 (2009).
[57] Y. Zhang, J.-P. Hu, B. A. Bernevig, X. R. Wang, X. C. Xie, and W. M. Liu, Phys. Rev. B **78**, 155413 (2008).
[58] A. Lherbier, B. Biel, Y.-M. Niquet, and S. Roche, Phys. Rev. Lett. **100**, 036803 (2008).
[59] C. F. F. Karney, Physica D **8**, 360 (1983).
[60] J. D. Meiss and E. Ott, Phys. Rev. Lett. **55**, 2741 (1985).
[61] J. D. Meiss and E. Ott, Physica D **20**, 387 (1986).
[62] Y.-C. Lai, M. Ding, C. Grebogi, and R. Blümel, Phys. Rev. A **46**, 4661 (1992).
[63] P. W. Brouwer, Ph.D. thesis, Leiden University, 1997.
[64] Y. Alhassid, Rev. Mod. Phys. **72**, 895 (2000).
[65] T. Guhr, A. Müller-roeling, and H. A. Weidenmüler, Phys. Rep. **299**, 189 (1998).
[66] H. U. Baranger and P. A. Mello, Phys. Rev. Lett. **73**, 142 (1994).
[67] R. A. Jalabert, J.-L. Pichard, and C. W. J. Beenakker, Europhys. Lett. **27**, 255 (1994).
[68] C. W. J. Beenakker, Rev. Mod. Phys. **69**, 731 (1997).
[69] R. Akis, D. K. Ferry, and J. P. Bird, Phys. Rev. Lett. **79**, 123 (1997).
[70] F. Aigner, S. Rotter, and J. Burgdörfer, Phys. Rev. Lett. **94**, 216801 (2005).
[71] R. G. Nazmitdinov, K. N. Pichugin, I. Rotter, and P. Šeba, Phys. Rev. B **66**, 085322 (2002).

[72] R. G. Nazmitdinov, H.-S. Sim, H. Schomerus, and I. Rotter, Phys. Rev. B **66**, 241302 (2002).
[73] L. Ying, L. Huang, Y.-C. Lai, and Y. Zhang, J. Phys.: Condens. Matter **25**, 105802 (2013).
[74] L. Ying, L. Huang, Y.-C. Lai, and C. Grebogi, Phys. Rev. B **85**, 245448 (2012).
[75] G.-L. Wang, L. Ying, Y.-C. Lai, and C. Grebogi, Phys. Rev. E **87**, 052908 (2013).
[76] L. M. Pecora, H. Lee, D. H. Wu, T. Antonsen, M. J. Lee, and E. Ott, Phys. Rev. E **83**, 065201 (2011).
[77] M. J. Lee, T. M. Antonsen, E. Ott, and L. M. Pecora, Phys. Rev. E **86**, 056212 (2012).
[78] W. H. Press, S. A. Teukolsky, W. T. Vetterling, and B. P. Flannery, *Numerical Recipes–The Art of Scientific Computing*, 3rd ed. (Cambridge University Press, Cambridge, UK, 2007).